



Influence of Different Abutment Designs on the Biomechanical Behavior of Dental Root-Analog Implant: A Three-Dimensional Finite Element Analysis

Ling He, PhD,* Deli Li, MD,† Jiwu Zhang, EB,‡§ Xiucheng Li, PhD,‡§ Songhe Lu, MD,¶|| and Zhihui Tang, MD||

Implant dentistry is constantly evolving toward simplification of clinical procedures and shortened treatment times, with such developments as immediate implant placement. Immediate implants are implants inserted immediately after surgical extraction of the teeth to be replaced.¹ The advantages of immediate implant placement are the decrease in treatment time and the avoidance of a second surgical intervention, leading to overall cost reduction and an improvement in the patients' psycho-

Objective: The aim of this study was to evaluate cross-sectional area of the abutments, strain distribution in the periimplant bone and dental root-analog implant by different abutment design under different loading conditions, through three-dimensional finite element analysis.

Methods: Two three-dimensional finite element models were established. Two types of abutments, oval cross section abutment (OCSA) and circular cross section abutment (CCSA) were designed, keeping the size of the thinnest implant wall 0.75 mm. Two types of load were applied to the abutment in each model: 100 N vertical load (V), 100 N vertical/50 N horizontal load (VH). The biomechanical behaviors of abut-

ments, implants, and periimplant bone were recorded.

Results: The cross-section area of OCSA is 36.5% larger than that of CCSA. In implants, the maximum von Mises stress value in OCSA design was 24.6% lower than that in CCSA design under V and under VH. In abutments, the maximum von Mises stress value in OCSA design was 40.0% lower than that in CCSA design under V, the maximum von Mises stress value in OCSA design was 12.2% lower than that in CCSA design under VH.

Conclusions and Clinical Significance: The irregular design offers advantages over regular design. (Implant Dent 2016;25:802–806)

Key Words: abutment design, dental root-analog implant, three-dimensional finite element analysis

*Assistant Researcher, Department of The Second Dental Center, Peking University School and Hospital of Stomatology & National Engineering Laboratory for Digital and Material Technology of Stomatology & Beijing Key Laboratory of Digital Stomatology, Beijing, People's Republic of China.

†Attending doctor, Department of The Second Dental Center, Peking University School and Hospital of Stomatology & National Engineering Laboratory for Digital and Material Technology of Stomatology & Beijing Key Laboratory of Digital Stomatology, Beijing, People's Republic of China.

‡Postgraduate, Department of School of mathematics and physical, University of Science & Technology Beijing, Beijing, People's Republic of China.

§Assistant Professor, Department of School of mathematics and physical, University of Science & Technology Beijing, Beijing, People's Republic of China.

¶Attending doctor, Department of The Second Dental Center, Peking University School and Hospital of Stomatology, Beijing, People's Republic of China.

||Professor, Chief of Department of The Second Dental Center, Department of The Second Dental Center, Peking University School and Hospital of Stomatology & National Engineering Laboratory for Digital and Material Technology of Stomatology & Beijing Key Laboratory of Digital Stomatology, Beijing, People's Republic of China.

Reprint requests and correspondence to: Zhihui Tang, MD, Department of The Second Dental Center, Peking University School and Hospital of Stomatology, No. 66 anliu, Chaoyang District, Beijing 100101, People's Republic of China, Phone: +86 10 82196237, Fax: +86 10 64907970, E-mail: tang_zhihui@live.cn

ISSN 1056-6163/16/02506-802

Implant Dentistry

Volume 25 • Number 6

Copyright © 2016 Wolters Kluwer Health, Inc. All rights reserved.

DOI: 10.1097/ID.0000000000000487

logical outlook for dental treatment.^{1,2} To obtain osseointegration, primary stability after implant placement is needed.^{1,2} For this reason, the surgical requirements for immediate implantation include extraction with careful preservation of the alveolar socket walls, and primary implant stability has been achieved by placing implants exceeding the alveolar apex by 3 to 5 mm, or by inserting implants of greater diameter than the remnant alveolus.^{1,2} The incon-

gruity between the socket wall and the endosseous implant shape remains, however, the major problem associated with immediate implant placement using conventional screw-type or cylinder-type implants.¹⁻⁴ This problem could be rectified by placing into the extraction sockets a custom-made root-analog implant (RAI), adapting the root to the extraction socket instead of adapting the bone to a preformed standardized implant. This approach could have

several advantages, such as uncomplicated immediate implant placement with decreased bone and soft tissue trauma and increased patient comfort.⁴

Recently, a novel approach to fabricate a custom-made titanium RAI has been proposed.^{3,5,6} With the combined use of Cone Beam Computed Tomography 3D data and high-end direct laser metal sintering (DLMS) technology, it was possible to manufacture a RAI with sufficient precision.^{3,5,6} In 2 different clinical reports, a custom-made, root-analog DLMS implant was placed into an extraction socket.^{5,6} A perfect congruence between implant and extraction socket was obtained; after 1 year of follow-up, the custom-made implants showed a perfect functional and esthetic integration.^{5,6} The reported abutments of RAI were integral, implants were nonsubmerged.⁷⁻⁹ Moreover, because of the irregular shape of RAI, regular abutment did not match it. However, irregular 2-piece abutment design for RAI has not been reported.

Therefore, the main goal of this study was to compare through three-dimensional finite element analysis (3D FEA) cross-sectional area, strain distribution in the periimplant bone, stress in the abutments and dental RAI by oval cross-section abutment (OCSA), and circular cross-section abutment (CCSA).

MATERIALS AND METHODS

Model Design

To obtain the geometry of a totally patient's canine, a computed tomography (CT) examination was performed on a volunteer, with approval from the ethical committee of Peking University School of Stomatology (PKUSSIRB-201522047). Her canine were scanned. The CT examination files were then imported into Ansys 15.0 (Ansys Corporation, Pittsburgh, PA). The dental RAI were chosen for this biomechanical analysis. The 3D geometries of the RAIs and abutments and bone were modeled in SolidWorks 2008 (SolidWorks Corporation, Ve' lizy-Villacoublay, France).

Two 3D FEA models, OCSA and CCSA were designed (Fig. 1), both keeping the size of the thinnest implant wall 0.75 mm. The abutments were both 4.5 mm lower than the platform of the implants, 5 mm higher than the platform

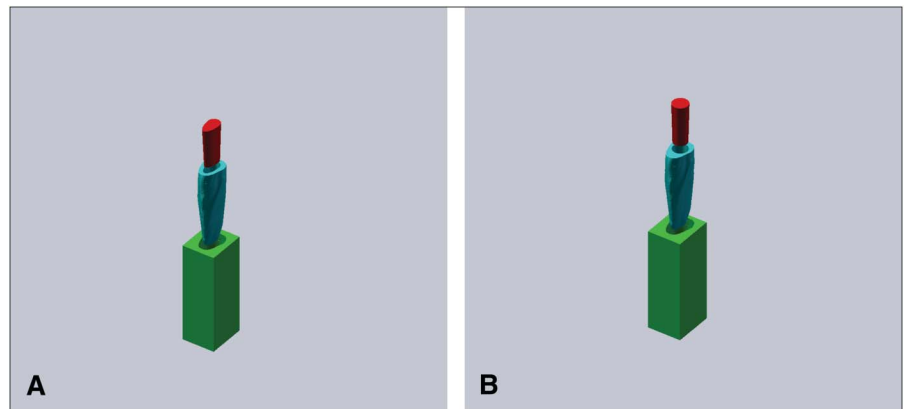


Fig. 1. The two 3D finite element models of the bone, RAI and abutments: (A) represents model A OCSA; (B) represents model B CCSA.

Table 1. Total Number of Elements and Nodes

	Elements	Nodes
Model A	1,118,716	190,064
Model B	1,063,736	181,132

of the implants, both with the taper 1.44 degrees. The geometries of the bone and implants and abutments were modeled and then meshed using Ansys 15.0 (Ansys Corporation, Pittsburgh, PA).

1. Model A, OCSA match RAI in the bone.
2. Model B, CCSA match RAI in the bone.

The models were meshed with 3D 4-node tetrahedron elements. The total numbers of elements and nodes are listed in Table 1.

Material Properties

The bone was composed of a 2-mm constant cortical bone layer around a cancellous bone core. The abutments and RAI were made of Ti-6Al-4V titanium alloy. The material properties of the cortical and cancellous bone, abutments, and implants were determined from values obtained from the literature (Table 2). All materials were

assumed to be isotropic, homogeneous, and linearly elastic.

Contact Management and Loading Conditions

The base of the block was fixed to prevent movements in all directions (x, y, z). It was assumed a perfect contact for all the interfaces by assigning "bonded" contact-type between the implant-bone and abutment-implant surfaces. The bonded contact-type is assigned when a perfect union between surfaces is desired, preventing the slip of one over the other or the separation of both. There was no surface penetration for the contacts.

Implants were considered totally osseointegrated, abutments were considered tightly touched. Therefore, a mechanically perfect interface was presumed to exist between implant and bone, abutment and implant.

The models were constrained at the nodes on the mesial and distal bone in all degrees of freedom. Two types of load were applied to the abutment in each model to simulate functional loading, namely 100 N vertical load, 100 N vertical/50 N horizontal load. To facilitate discussion, the 2 loading conditions have been abbreviated as V and VH for vertical load and vertical/horizontal load.

Table 2. Material Properties

	Young Modulus (megapascal, MPa)	Poisson Ratio	Reference
Ti-6Al-4V	103,400	0.35	Sertgöz and Güvener ¹⁰
Cortical bone	13,700	0.3	Barbier et al ¹¹
Cancellous bone	1370	0.3	Barbier et al

Table 3. Cross-Section Area of Abutment

Abutment Design	OCSA	CCSA
Area (mm ²)	17.1444	12.56

Table 4. Maximum von Mises Strains in Periimplant Bone Under 2 Loading Conditions (μ ϵ)

Loading Condition	Model A	Model B
V	244	283
VH	244	283

Table 5. Maximum von Mises Stresses in Implant Under 2 Loading Conditions (MPa)

Loading Condition	Model A	Model B
V	14.579	19.3398
VH	14.579	19.3249

RESULTS

Cross-Section Area of Abutment

Cross-section area of abutment for each model is shown in Table 3. For dental RAI, keeping the size of the thinnest wall 0.75 mm, the cross-section area of OCSA is 36.5% larger than that of CCSA.

Strain in Periimplant Cortical Bone

Maximum von Mises strains in peri-implant cortical bone under 2 types of load for each model is shown in Table 4. Under all 2 loading conditions, the maximum strain values were below 2500 μ ϵ in all models. In model A, the peak strain values in the cortical bone were lower than that in model B. However, in model A, the maximum strain value under V was as high as that under VH, in model B, the maximum strain value under V was also as high as that under VH.

Stress Distribution in Implants

The maximum von Mises stress values in the implants under 2 loading conditions in each model are shown in Table 5. Stress distributions in the implant of each model under 2 loading conditions are illustrated in Figures 2 and 3. It was notable that, the maximum von Mises stress value in model A was 24.6% lower than that in model B under V, the maximum von Mises stress value in model A was 24.6% lower than that in

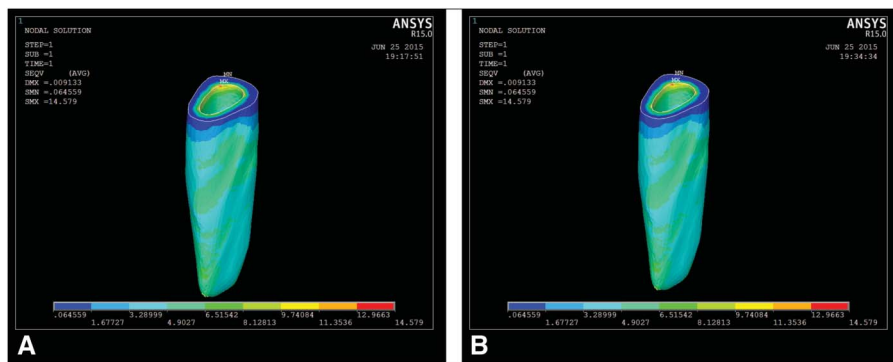


Fig. 2. Maximum von Mises stress distribution in the implant of model A under 2 loading conditions ((A) V, (B) VH). Model A: OCSA matched RAI. **A**, When 100 N vertical load is imposed, stress distribution in the implant is expressed as different colors, blue represents low stress value and red represents high stress value. The stress around the implant platform is basically homogeneous (dark blue). The maximum von Mises stress of the implant is 14.579 MPa. **B**, When 100 N vertical/50 N horizontal load was imposed, stress distribution in the implant is expressed as different colors, blue represents low stress value and red represents high stress value. The stress around the implant platform is basically homogeneous (dark blue). The maximum von Mises stress of the implant is 14.579 MPa.

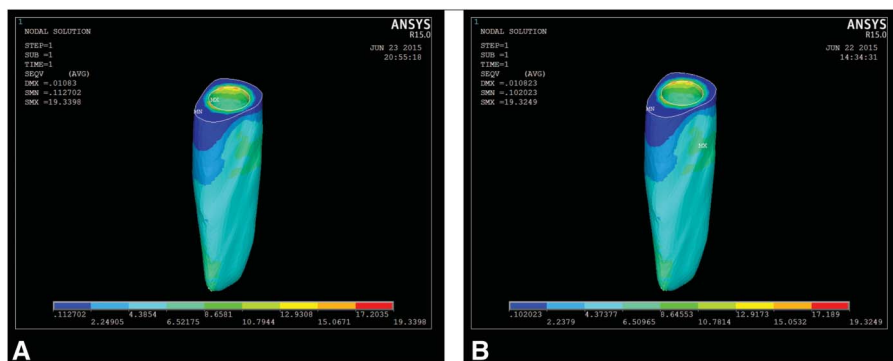


Fig. 3. Maximum von Mises stress distribution in the implant of model B under 2 loading conditions ((A) V, (B) VH). Model B: CCSA matched RAI. **A**, When 100 N vertical load is imposed, stress distribution in the implant is expressed as different colors, blue represents low stress value and red represents high stress value. The stress around the implant platform is obviously nonhomogeneous (dark blue). The maximum von Mises stress of the implant is 19.3398 MPa. **B**, When 100 N vertical/50 N horizontal load was imposed, stress distribution in the implant is expressed as different colors, blue represents low stress value and red represents high stress value. The stress around the implant platform is obviously nonhomogeneous (dark blue). The maximum von Mises stress of the implant is 19.3398 MPa.

Table 6. Maximum von Mises Stresses in Abutment Under 2 Loading Conditions (MPa)

θ Loading Condition	Model A	Model B
V	16.6364	27.7487
VH	16.6364	18.9385

model B under VH. The maximum von Mises stress values both located on the platform interface between the abutment and implant in model A and in model B.

Stress Distribution in Abutments

The maximum von Mises stress values in the abutments under two loading conditions in each model are shown in Table 6. Stress distributions in the abutment of each model under 2 loading conditions are illustrated in Figures 4 and 5. It was notable that the maximum von Mises stress value in model A was 40.0% lower than that in model B under V, the maximum stress value in model A was 12.2% lower than that in model B under VH. The maximum von Mises stress values are both located on the

40.0% lower than that in CCSA design under V, the maximum von Mises stress value in OCSA design was 12.2% lower than that in CCSA design under VH.

Therefore, the OCSA design offer advantages over CCSA design in RAI. The OCSA design could be a feasible choice for RAI. The 3D FEA method described in this work is an important tool to predict the stress distribution, assisting on structural design of abutments.

However, owing to the scarcity of literature concerning the abutment design of RAI on stress distribution in the abutment and in the implant, further experimental stress analysis and long-term clinical research needs to be performed.

CONCLUSION

Within the limitations of this *in vitro* study, the following conclusions can be drawn:

1. The maximum von Mises strain values in periimplant bone were within physiological limits in both 2 models.
2. Oval abutment matches the irregular shape of dental RAI, which leads to the abutment bigger than regular circular abutment.
3. The stress in oval abutment is lower than that in circular abutment, which leads to the oval abutment more durable.
4. Oval abutment design is essential for irregular RAI.

DISCLOSURE

The study was supported by the Beijing Municipal Science and technology project, project number: Z151100003715007.

The authors claim to have no financial interest, either directly or indirectly, in the products or information listed in the article.

L. He and D. Li both contributed equally.

APPROVAL

Approval from the ethical committee of Peking University School of Stomatology (PKUSSIRB-201522047).

REFERENCES

1. Koh RU, Rudek I, Wang HL. Immediate implant placement: Positives and negatives. *Implant Dent*. 2010;19:98–108.
2. Kazor CE, Al Shamari K, Sarment DP, et al. Implant plastic surgery: A review and rationale. *J Oral Implantol*. 2004;30:240–254.
3. Moin DA, Hassan B, Mercelis P, et al. Designing a novel dental root analogue implant using cone beam computed tomography and CAD/CAM technology. *Clin Oral Implant Res*. 2011. doi:10.1111/j.1600-0501.2011.02359.x.
4. Regish KM, Sharma D, Prithviraj DR. An overview of immediate root analogue zirconia implants. *J Oral Implant*. 2011;10-00208. doi:10.1563/AAIDD-10-00208.
5. Figliuzzi M, Mangano F, Mangano C. A novel root analogue dental implant using CT scan and CAD/CAM: Selective laser melting technology. *Int J Oral Maxillofac Surg*. 2012;41:858–862.
6. Mangano FG, Cirotti B, Sammons RL, et al. Custom-made, root-analogue direct laser metal forming implant: A case report. *Lasers Med Sci*. 2012;27:1241–1245.
7. Mangano FG, Franco MD, Caprioglio A, et al. Immediate, non-submerged, root-analogue direct laser metal sintering (DLMS) implants: A 1-year prospective study on 15 patients. *Lasers Med Sci*. 2014;29:1321–1328.
8. Pirker W, Wiedemann D, Lidauer A, et al. Immediate, single stage, truly anatomic zirconia implant in lower molar replacement: a case report with 2.5 years follow-up. *Int J Oral Maxillofac Surg*. 2011;40:212–216.
9. Pirker W, Kocher A. Immediate, non-submerged, root-analogue zirconia implants placed into single-rooted extraction sockets: 2-year follow-up of a clinical study. *Int J Oral Maxillofac Surg*. 2009;38:1127–1132.
10. Sertgöz A, Güvener S. Finite element analysis of the effect of cantilever and implant length on stress distribution

in an implant-supported prosthesis. *J Prosthet Dent*. 1996;76:165–169.

11. Barbier L, Vander Sloten J, Krzesinski G, et al. Finite element analysis of non-axial versus axial loading of oral implants in the mandible of the dog. *J Oral Rehabil*. 1998;25:847–858.

12. Tepper G, Haas R, Zechner W, et al. Three-dimensional finite element analysis of implant stability in the atrophic posterior maxilla: A mathematical study of the sinus floor augmentation. *Clin Oral Implant Res*. 2002;13:657–665.

13. Frost HM. Bone “mass” and the “mechanostat”: A proposal. *Anat Rec*. 1987;219:1–9.

14. Liu JY, Pan SX, Dong J, et al. Influence of implant number on the biomechanical behavior of mandibular implant-retained/supported overdentures: a three-dimensional finite element analysis. *J Dent*. 2013;41:241–249.

15. Dittmer S, Dittmer MP, Kohorst P, et al. Effect of implant-abutment connection design on load bearing capacity and failure mode of implants. *J Prosthodont*. 2011;20:510–516.

16. Tabata LF, Rocha EP, Barao VA, et al. Platform switching: Biomechanical evaluation using three-dimensional finite element analysis. *Int J Oral Maxillofac Implants*. 2011;26:482–491.

17. Natali AN, Pavan PG, Ruggero AL. Analysis of bone-implant interaction phenomena by using a numerical approach. *Clin Oral Implant Res*. 2006;17:67–74.

18. Petrie CS, Williams JL. Comparative evaluation of implant designs: Influence of diameter, length, and taper on stains in the alveolar crest. A three-dimensional finite-element analysis. *Clin Oral Implant Res*. 2005;16:486–494.

19. Hudieb MI, Wakabayashi N, Kasugai S. Magnitude and direction of mechanical stress at the osseointegrated interface of the microthread implant. *J Periodont*. 2011;82:1061–1070.

20. Chang CL, Chen CS, Hsu ML. Biomechanical effect of platform switching in implant dentistry: A three-dimensional finite analysis. *Int J Oral Maxillofac Implants*. 2010;25:295–304.

21. Danza M, Carinci F. Bone platform switching: A retrospective study on the slope of reverse conical neck. *Quintessence Int*. 2010;41:35–40.